Application of the SKYRAD Improved Langley plot method for the *in situ* calibration of CIMEL Sun–sky photometers

Monica Campanelli, Víctor Estellés, Claudio Tomasi, Teruyuki Nakajima, Vincenzo Malvestuto, and José Antonio Martínez-Lozano

The *in situ* procedure for determining the solar calibration constants, originally developed for the PREDE Sun–sky radiometers and based on a modified version of the Langley plot, was applied to a CIMEL instrument located in Valencia, Spain, not integrated into AERONET. Taking into account the different mechanical and electronic characteristics of the two radiometers, the method was adapted to the characteristics of the CIMEL instrument. The iterative procedure for the determination of the solar calibration constants was applied to a 3-year data set. The results were compared with the two sets of experimental calibration constants determined during this period using the standard Langley plot method. The agreement was found to be consistent with the experimental errors, and the method can definitely also be used to determine the solar calibration constant for the CIMEL instrument, improving its calibration. The method can be used provided the radiometer is previously calibrated for diffuse radiance using a standard lamp.

OCIS codes: 010.1290, 010.1110.

1. Introduction

Atmospheric aerosols have an important effect on the Earth's climate forcing, causing marked inhomogeneities over space and time scales in the distribution of the Earth's global radiation balance. Such discrepancies need to be more appropriately characterized through the simultaneous use of remote sensing and ground-based Sun-photometric measurements.[1] Several international networks of ground-based photometers have been set up over the past 20 years, taking advantage of the development of new instruments and techniques. Two of these networks are the SKYNET network[2] and the AERONET network.[3]

SKYNET consists of more than 20 sites mainly located in Asia. Its standard sky–Sun photometer is a PREDE POM sky radiometer whose data are processed using the public domain inversion code known as SKYRAD.[4,5] AERONET is distributed mainly in North America and Europe and employs the CIMEL CE318 sky–Sun photometer as the standard instrument. More than 200 units take part in the AERONET program, which adopts an original inversion code to analyze the measurements.[6,7] The simultaneous study of the databases from both networks offers a global picture of the atmospheric aerosol properties: the more widespread these networks are on the Earth, the better the picture that will be achieved to elucidate the climate prognoses.

According to World Meteorological Organization (WMO) guidelines,[8] only data provided by recognized international networks should be used in aerosol climatology studies, since they alone can ensure well-tracked calibration procedures and data quality standards. SKYNET and AERONET are therefore both suitable for yielding reliable data. The AERONET calibration procedure is defined by a stringent protocol.[3] Field instruments must be periodically sent to the NASA Goddard Space Flight Center in Maryland, USA or Lille University, France, for calibration through intercomparison with reference instruments.

M. Campanelli (m.campanelli@isac.cnr.it) and V. Malvestuto are with the Institute of Atmospheric Sciences and Climate, Italian National Research Council, Via Fosso del Cavaliere, 100, Roma Tor Vergata, I-00133, Italy. V. Estellés and J. A. Martínez-Lozano are with the Departamento Termodinámica of the Facultat de Física, Universitat de València, c/Dr. Moliner, 50 46100 Burjassot, Spain. C. Tomasi is with the Institute of Atmospheric Sciences and Climate, Italian National Research Council, Via Gobetti 101, Bologna, I-40129, Italy. T. Nakajima is with the Center for Climate System Research, The University of Tokyo 5-1-5 Kashiwanoha, Kashiwa, Chiba 277-8568, Japan.

Received 30 August 2006; revised 18 December 2006; accepted 20 December 2006; posted 10 January 2007 (Doc. ID 74604); published 23 April 2007.

0003-6935/07/142688-15$15.00/0

The periodicity is nominally stated to be 6 months, although periods of 1 year are not unusual. The annual return of the equipment not only allows the calibration but also provides an important opportunity to maintain the equipment, including changing filters, when required. However, the calibration status is checked only once a year, and hence the appropriate correction to data can only be applied *a posteriori*, through a re-elaboration of the corrected data. An additional problem is that the numerous instruments participating in the network imposes the need for supplementary manpower, implying higher costs. Therefore this well-planned calibration protocol is a major activity, which considerably limits the expansion capacity of the network, bearing in mind that some 240 CIMEL instruments now operate officially within AERONET, while a further 250 examples are working outside of it.[9] The consequence is that a great amount of globally distributed data are in practice not utilized to reach a more exhaustive and extended aerosol climatology assessment over the global scale.

Conversely, SKYNET adopts an *in situ* uncentralized calibration procedure that allows operators to track and evaluate the calibration status on a continuous basis,[10] keeping the periodic check mostly for maintenance reasons and offering the advantage of reducing the overall cost. In this way, the data gaps incurred by the periodical shipments are considerably reduced, and the likelihood of instrumental damages attributable to transport also decreases. However, this *in situ* method can thus far be correctly employed only on PREDE instrumentation.

The method, hereinafter referred to as SKYIL (SKYRAD Improved Langley plot), retrieves the solar calibration constant by means of a modified version of the Langley plot.[10] The calibration value is retrieved by fitting the natural logarithm of the direct solar irradiance versus the product of the relative optical air mass and the total extinction optical thickness, as retrieved by the SKYRAD code, instead of only the air mass as occurs with the standard Langley plot.[11] The results obtained applying SKYIL to PREDE field measurements have provided estimates of the precision in determining the solar calibration constant ranging from 1% to 2.5%, depending on wavelength.[10]

The aim of the present paper is to apply the SKYIL method to a CIMEL sky–Sun photometer. A calibration method independent of the AERONET system would be very useful for diagnosing the condition of a sky radiometer, whose data analysis is very vulnerable to small errors in the measured data. Using an independent method, the variation of the calibration constant owing to instrumental drift can be quickly spotted and the appropriate corrections to data applied starting exactly from the period in which the deviation occurred.

At present, the instrument used in the present analysis does not belong to AERONET, although it has recently been included in RIMA (Red Ibérica de Medida de Aerosoles), a network of CIMEL CE318 sky–Sun photometers being set up in Spain. Therefore access to raw data, calibration process, and EPROM user programming were available for the present study.

2. Instrument Database and Calibration

The SKYIL method was applied to the CIMEL Sun–sky radiometer, model CE318-2 (serial number 176), belonging to the Solar Radiation Group of the University of Valencia, Spain. This model is equipped with an eight-filter wheel having peak transmission wavelengths of 440, 670, 870, and 1020 nm. A channel centered on a strong water vapor absorption band (940 nm) is used for the retrieval of the columnar water vapor content, and three plastic polarizers are installed to take polarization measurements at 870 nm. The instrument automatically measures direct solar and sky diffuse irradiance following a standard schedule,[3] resulting in the retrieval of 8–10 almucantar scenarios per day. However, up to 26 user scenarios can be added to retrieve more daily almucantar measurements. When implemented, instrument No. 176 was capable of measuring a daily number of more than 30 almucantar scenarios.

The Sun photometer was deployed in January 2002 in Burjassot, Spain, and has been working at this site almost continuously. The site (latitude 39.508°, longitude 0.418°, altitude 60 m above sea level (ASL)) is on the Spanish Mediterranean coast, located in the suburbs of Valencia (total population of 1.5 million). Due to its proximity to Valencia (5 km northwest) and the Mediterranean shore (10 km west), it is characterized by the continuous presence of local anthropogenic and marine aerosols. Air masses from northern Africa frequently arrive over the site, mainly in the summer season. This renders the site clearly unsuitable for the application of the standard Langley plot method for calibration purposes, since the numerous aerosol sources can increase the daily variability of the aerosol burden.

The data set used in the present work consists of measurements taken from January 2002 to March 2005, only in the almucantar geometry.[12] To ensure that measurements were not affected by clouds, a cloud screening was performed according to the following steps: (i) a symmetry test of the radiance measured at several zenith angles, on both sides of the solar disk, as described by Holben *et al.*[3]; (ii) the rejection of the complete almucantar in all cases where none of the data points, for angles smaller than 7°, respect the symmetry test of the above criterion; this step is important because this region is crucial for an accurate inversion of the radiance data; (iii) the screening algorithm described by Smirnov *et al.*,[13] applied to measurements of direct solar irradiance. Applying the cloud screening procedure to measurements taken at the above-mentioned wavelengths, it is difficult to recognize high thin clouds or spatially homogeneous stratus. Therefore the presence of such clouds cannot be definitely excluded.[13] Further details on the characterization of the aerosol properties at this site can be found elsewhere.[14,15]

Throughout the period, the instrument calibration constants were regularly checked, for both direct and diffuse irradiance measurements. The methods and the results are described in the following subsections.

A. Direct Irradiance Calibration

The first set of calibration constants (11 July 2002) for direct solar irradiance measurements was retrieved through intercomparison with a reference instrument, the CIMEL CE318 (serial number 307), operating during a field campaign in Sierra Nevada, Spain, at a site above 2300 m ASL.[16] This master instrument was calibrated by applying the standard Langley plot method to such measurements performed over 16 days in July 2002. Additional details of the calibration procedure are provided in other papers.[12,15]

The second set of calibration constants (25 October 2004) was obtained through an intercomparison transfer test employing another reference instrument, the CIMEL model CE318NE (serial number 430), performing simultaneous measurements on several clear-sky days of October 2004, in Valencia. The reference instrument was calibrated using the standard Langley plot, applied to a database of measurements taken from 24 April to 12 July 2004 at Aras de los Olmos, Spain, a mountain site located at 1300 m ASL and 100 km away from anthropogenic sources. The resulting calibration values (V_0^{exp}) and their estimated percentage uncertainty [$\varepsilon_T(\%)$] are shown in Table 1. The parameter ε_T is given as the sum of the Langley uncertainty, evaluated as the standard deviation (STD) over the entire data set of the calibration values retrieved at Aras de los Olmos, and the uncertainty obtained from the transfer ratio itself, evaluated as the STD over the days of simultaneous measurements. The outliers were removed following the Chauvenet criterion.[17] Compared with the nominal calibration uncertainties provided by the AERONET-related literature for field instruments[3] (1%–2%), the values obtained here are somewhat higher. The reason could be the different conditions of the calibration performed for the master instruments. In fact, AERONET master Sun–sky radiometers are calibrated at Mauna Loa, Hawaii, a remote site in the middle of the Pacific Ocean, with an accuracy of 0.2%–0.5%.[3] The present master instruments were calibrated instead at continental sites, often strongly affected by the arrival of European and African air masses. Therefore their calibration uncertainty [$\varepsilon_m(\%)$], given in Table 1, is rather higher than expected and propagates to the field instruments.

Table 1. Spectral Solar Calibration Constants as Retrieved by the Standard Langley Plot with the Estimated Uncertainty for the Master Instruments (ε_m) and for the Field Instruments (ε_T) after the Intercomparison Transfer Test

	11 July 2002			25 October 2004		
λ (nm)	V_0^{exp}	$\varepsilon_m(\%)$	$\varepsilon_T(\%)$	V_0^{exp}	$\varepsilon_m(\%)$	$\varepsilon_T(\%)$
440	2761	0.7	1.1	2836	1.8	2.4
670	9129	0.4	0.9	9123	0.9	1.4
870	5218	0.5	0.9	5070	0.8	1.3
1020	2822	0.6	1.1	2802	0.8	1.2

B. Lamp Calibration of Diffuse Radiance

The diffuse radiance calibration is generally obtained by measuring the exit radiance of a previously calibrated integrating sphere. It was performed approximately every six months, throughout the whole measurement period. A set of four lamps was employed over different spectral intervals and for various illuminance levels during the period: (i) a Li-Cor calibrator unit with an adaptor for radiance, (ii) two Bentham integrating spheres, and (iii) an Optronic OL-455 integrating sphere. The details of the calibration procedure are described by Estelles.[12] The uncertainty of the exit radiance of each integrating sphere is obviously different for each manufacturer, although it also depends on their temporal degradation (mainly related to the numbers of hours of instrumental use). A new Bentham lamp is claimed to have a 2% radiance uncertainty from 380 to 800 nm, increasing up to 5% at 1100 nm. The CIMEL calibration session was performed after a few hours of use of the two lamps. The Optronic lamp is claimed to be more accurate, but it accumulated a great number of measurement hours before the calibration session and the uncertainty was estimated consequently to rise to roughly 5%. Therefore a propagated 5% nominal uncertainty was assumed for the CIMEL radiance calibration. Figure 1 shows the evolutionary patterns of the calibration constants throughout the 2003–2005 period. The calibration values determined using the Optronic OL source are given in Fig. 1, separately from those simultaneously obtained using the two Bentham lamps (unit No. 4884 in the 2003 session and No. 7281 in that of 2005), to check the performances of the lamps. The calibration time patterns give evidence of an annual decrease in the radiance calibration constant

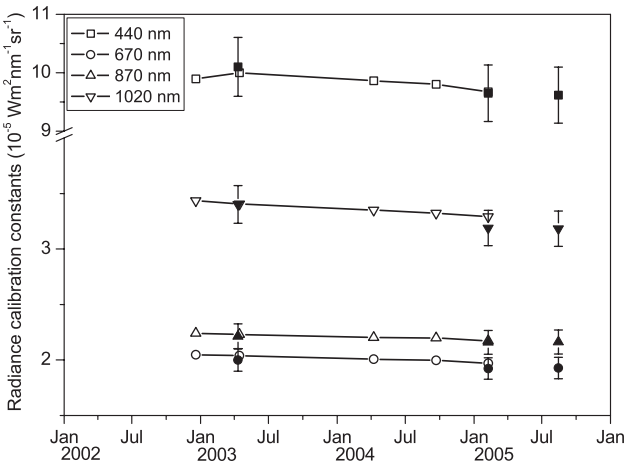

Fig. 1. Evolutionary time patterns of the radiance calibration constant values throughout the 2002–2005 period. Open symbols refer to the calibration constants obtained using the Optronic OL lamp, and solid symbols refer to the simultaneous calibration values obtained with the Bentham SRS8 lamps. The error bars define a 5% uncertainty value.

values equal to −1.1%, −1.8%, −1.5%, and −2.0% for the 440, 670, 870, and 1020 nm channels, respectively. No optical parts of the instrument were substituted or renewed during the calibration period examined in Fig. 1.

3. Method

As mentioned above, the application of the SKYIL method[10] is based on the use of the SKYRAD code. The method retrieves the spectral values of the solar calibration constant $V_0(\lambda)$ at various wavelengths λ, through a best-fit procedure of $\ln V(\lambda)$ plotted versus $m_0\tau(\lambda)$, based on the following:

$$\ln V(\lambda) = \ln V_0(\lambda) - m_0\tau(\lambda), \tag{1}$$

where $V(\lambda)$ is the measured direct solar irradiance, $m_0 = 1/\cos\theta_0$ is the inverse of the cosine of the solar zenith angle θ_0, and $\tau(\lambda)$ is the total extinction optical thickness calculated by the inversion procedure of the forward-scattering sky radiance data, performed using the SKYRAD code.

In particular, the quantity used in the inversion is the normalized radiance $R(\lambda, \Theta)$ defined as follows:

$$R(\lambda, \Theta) = \frac{E(\lambda, \Theta)}{\Delta\Omega(\lambda)V(\lambda)m_0} = \frac{L(\lambda, \Theta)}{V(\lambda)m_0}, \tag{2}$$

where $E(\lambda, \Theta)$ is the solar diffuse irradiance measured by the instrument at several scattering angles Θ, $\Delta\Omega(\lambda)$ is the solid view angle of the instrument optics, and $L(\lambda, \Theta) = E(\lambda, \Theta)/\Delta\Omega(\lambda)$ is the corresponding radiance.

This calibration method was developed for the PREDE instruments, where both direct and diffuse irradiance can be measured using the same sensor. Normalized radiance $R(\lambda, \Theta)$ can be calculated using the above quantities in measured count units, thus eliminating the need for further calibrations. Whenever the technique is applied to the CIMEL sky–Sun photometers, it must be taken into account that $V(\lambda)$ and $E(\lambda, \Theta)$ are measured by two different sensors, and hence the ratio $R(\lambda, \Theta)$ in Eq. (2) cannot be correctly defined in terms of these two quantities given in count units. To express the above quantities in absolute radiance units (W/m^2), it is useful to employ a lamp calibration for calculating the diffuse radiance $L(\lambda, \Theta)$ and to express $V(\lambda)$ in terms of the radiance units of $F(\lambda)$ given by

$$F(\lambda) = \frac{V(\lambda)}{V_0(\lambda)} F_0(\lambda), \tag{3}$$

where $F_0(\lambda)$ ($Wm^{-2}nm^{-1}$) is the incoming solar irradiance at the top of the atmosphere, obtained from the SMARTS2 model.[18] This model applies some improvements to the extraterrestrial spectrum[19] and was convoluted with the CIMEL experimental transmissivity filter functions to retrieve a reliable irradiance value for each channel. To apply the SKYIL method to CIMEL instruments, using Eqs. (2) and (3), it is convenient to first assume a preliminary value of solar calibration constant $V_0(\lambda)$ as a first guess, retrieved, for example, by the standard Langley plot technique. Subsequently, the iterative method shown in Fig. 2 can be applied by first determining $F(\lambda)$ in terms of Eq. (3), using a first guess for $V_0(\lambda)$, indicated as $V_0^0(\lambda)$, and then calculating $R(\lambda, \Theta)$. From the inversion of this quantity, $\tau(\lambda)$ is retrieved and inserted into Eq. (1) to derive a first estimate of $V_0(\lambda)$ [indicated as $V_0^1(\lambda)$], which is in turn used to recalculate $F(\lambda)$ and $R(\lambda, \Theta)$ and to retrieve $\tau(\lambda)$. Thereupon the improved Langley plot is again applied to estimate $V_0(\lambda)$. The loop is stopped at the nth iteration, when the difference between $V_0^{n-1}(\lambda)$ and $V_0^n(\lambda)$ is found to be lower than 2.5%, or the number of iterations exceeds ten. Each final retrieved value is adopted as a first guess for the following day or for the calculation of the evening value of the same day, since the method permits the determination of two values of $V_0(\lambda)$ each day, the former relative to the morning, the latter to the evening. The threshold value of 2.5% was chosen because it defines the accuracy of the method retrieved by Campanelli *et al.*[10]

4. Results

The data set was processed using as a first guess the calibration values determined in July 2002 (Table 1). The values of $V_0(\lambda)$ obtained for a SKYRAD code inversion accuracy lower than 5% were rejected according to the selection criteria established by Campanelli *et al.*[10] A quality check was also applied to the fit of $\ln V_0(\lambda)$ versus $m_0\tau(\lambda)$, which consists of the following steps: (i) only the measurements taken for $m_0 < 4.5$ were selected; (ii) a minimum number of four points was used, providing that they were at least half of the total number of available points; (iii) the difference between the maximum and the minimum value of $\ln(m_0\tau(\lambda))$ was required to be greater than 0.5; and (iv) a fit was performed using only the measurements whose vertical distance from the trend does not exceed the corresponding residual standard deviation.

In all cases where $\tau(500\text{ nm}) > 0.3$, $V_0(\lambda)$ was found to have a significant dependence on the imaginary part k of the particulate refractive index that is assumed in the SKYRAD code inversion.[10] Since an incorrect value of k yields an unreliable value of $V_0(\lambda)$, a quality check was performed, rejecting all the values of $V_0(\lambda)$ found for $\tau(440\text{ nm}) > 0.3$, measurements not being available at the 500 nm wavelength.

Following the procedure defined by Campanelli *et al.*[10] to filter the outliers and short-term variations related to the method itself, the Chauvenet criterion[17] was adopted and a three-point moving average technique was applied to the series of $V_0(\lambda)$ obtained after the rejection of all cases with high values of the optical thickness. Figure 3 shows the results after the quality check. The accuracy of the method in terms of the internal consistency of the retrieved values of $V_0(\lambda)$ was estimated by the dispersion of the values with respect to the regression line of each series.

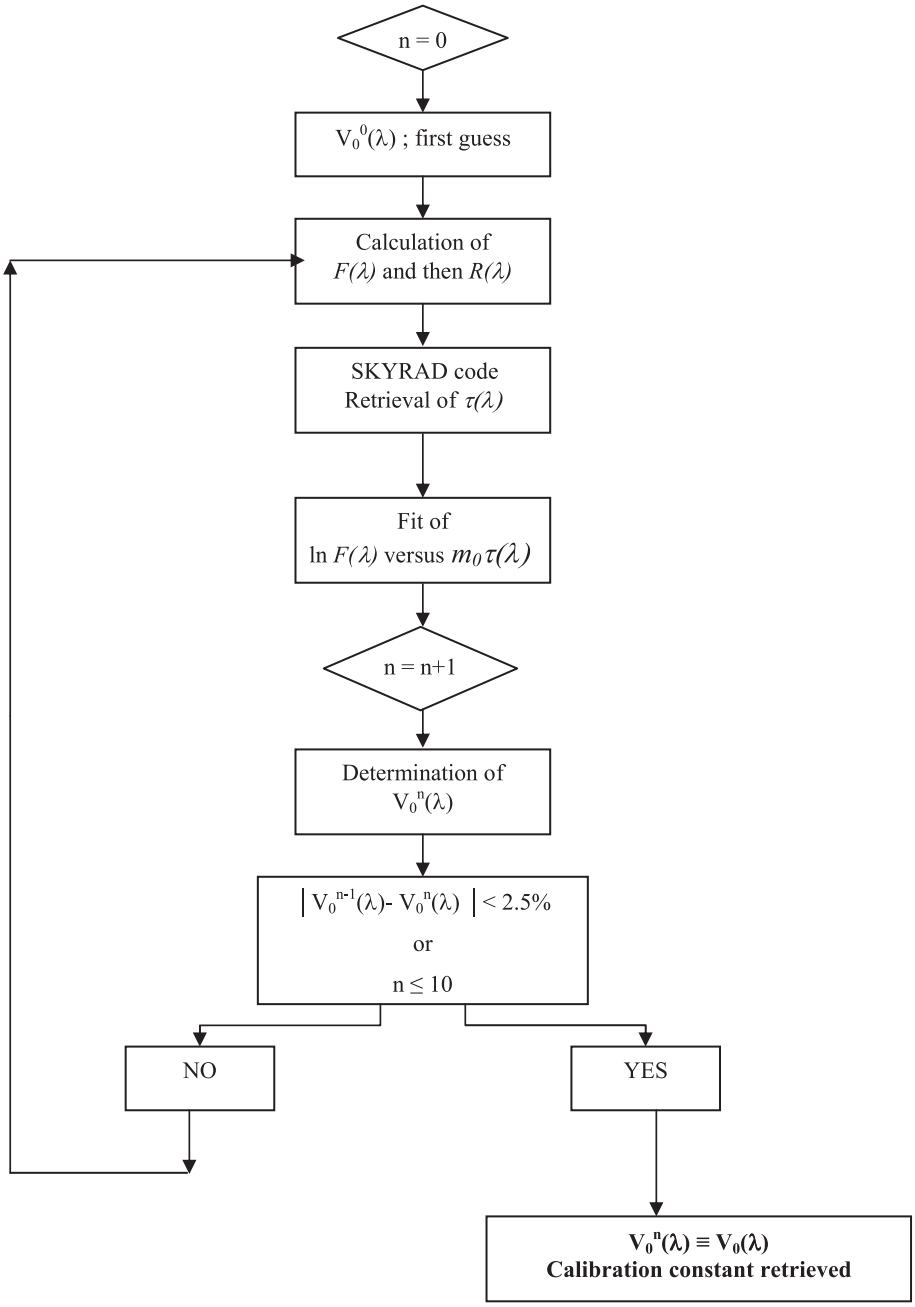

Fig. 2. Iterative method for the calculation of the solar calibration constant using the SKYIL method for a CIMEL instrument.

Percentage values of accuracy are given in Table 2, where they are also compared with those retrieved by Campanelli *et al.*[10] for the PREDE instrument using the same SKYIL method. Table 2 shows that an appreciably improved accuracy was achieved in the present results at all the wavelengths with respect to the previous ones.[10] This improvement is substantially due to (i) the rejection of the data corresponding to high optical thickness values, while this selection was not made in the procedure followed by Campanelli *et al.*,[10] and (ii) the adoption of the Chauvenet criterion[17] imposing more restricted limits than those proposed by Campanelli *et al.*,[10] where only the points lying beyond the 3σ distance were discarded, σ being the standard deviation calculated over the entire data set. In fact, the calibration constant values were monitored in the present procedure on a daily basis, and not only at the end of the analysis of the entire three-year data set, as done in Campanelli *et al.*[10] Through this step, each calibration value provided by the SKYIL method and lying far from the mean by more than 3σ was rejected, the values of σ and the mean being calculated over the whole set of calibration points within a time interval of 60 days, providing that the above set included at least five calibration points. In this way the data set turned out to be better filtered, and the dispersion of the results was appreciably limited.

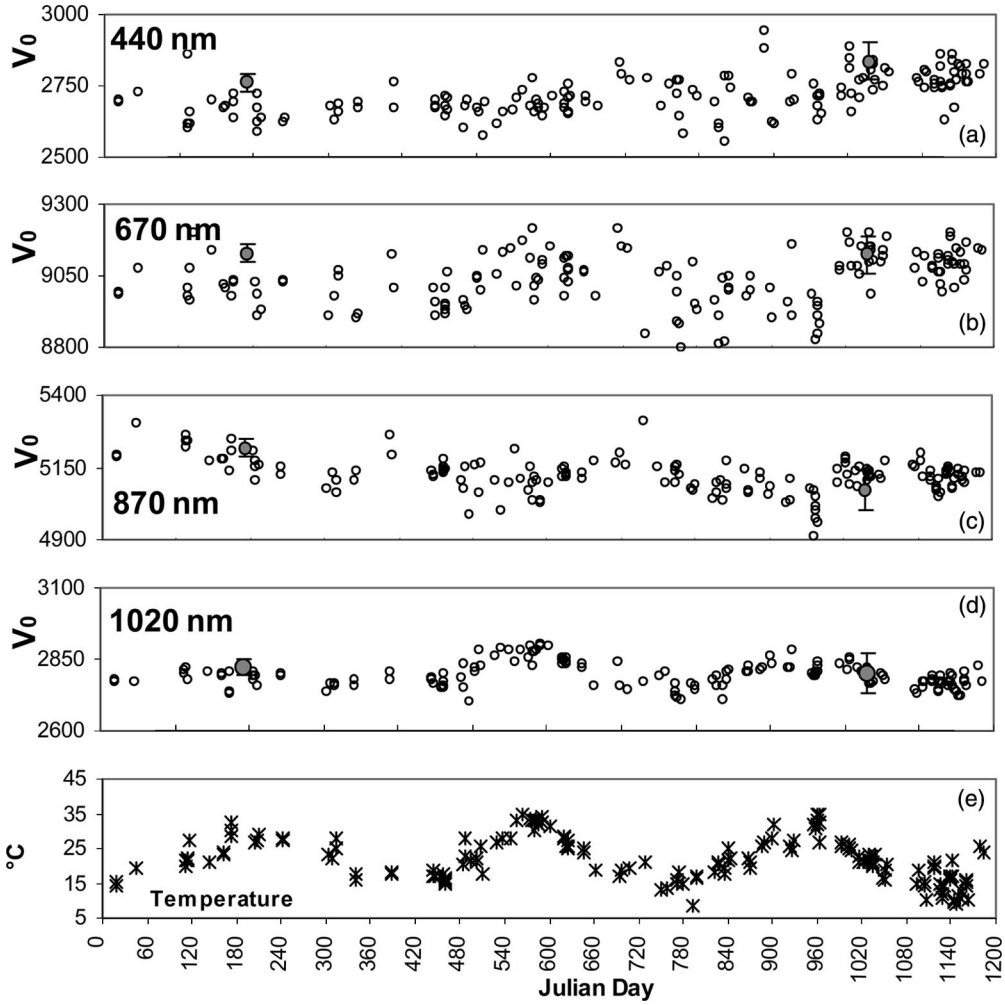

Fig. 3. Time patterns of the calibration constants $V_0(\lambda)$ at the four wavelengths, obtained after the quality selection: (a), (b), (c), and (d) refer to λ = 440, 670, 870, and 1020 nm, respectively. Gray points with error bars give the experimental calibration values of $V_0^{exp}(\lambda)$. (e) Time patterns of the temperature inside the instrument. The origin of the Julian day axis is set at 1 January 2002.

The improvement of accuracy with respect to the previously retrieved values[10] is an important result, since the nominal uncertainty on the values of $V_0(\lambda)$ given by the AERONET calibration method (of 1%–2%) and the uncertainty of the SKYIL method turned out to be more similar in the present case, although they could not be properly compared because neither of them are absolute estimates.

Table 2. Accuracy of the SKYIL Method in Retrieving $V_0(\lambda)$ at the Four Wavelengths

	Accuracy of the $V_0(\lambda)$ Retrieval (%)			
Present case	440 nm	670 nm	870 nm	1020 nm
Before temperature correction	2.3	1.2	1.1	1.5
After temperature correction	2.2	1.2	0.9	1.0
Campanelli *et al.* (Ref. 10)	400 nm	500 nm	870 nm	1020 nm
	2.5	2.0	1.8	2.0

A preliminary examination of the features shown in Figs. 3(a), 3(b), 3(c), and 3(d) clearly reveals the occurrence of an oscillation of $V_0(\lambda)$ over a period of approximately one year, particularly marked at 1020 nm. Comparing this behavior with the temperature time patterns shown in Fig. 3(e) and measured by a sensor placed inside the head of the instrument, where both sensor and filters are housed, the oscillation seemed to have the same tendency. Thus a specific analysis of the temperature dependence was required, considering that (i) the SKYIL method does not include a similar study since the PREDE instrument is thermostated, and (ii) a marked influence of the external temperature of the CIMEL on the output signals and, hence, on the determination of the calibration constants $V_0(\lambda)$, is expected to occur, since this CIMEL example is not housed in a thermostated box. Therefore it is reasonable to assume that the measurements taken by the sensor are subject to marked drift effects related to the inner temperature, which depend closely on wavelength, while the transmission peak wavelength

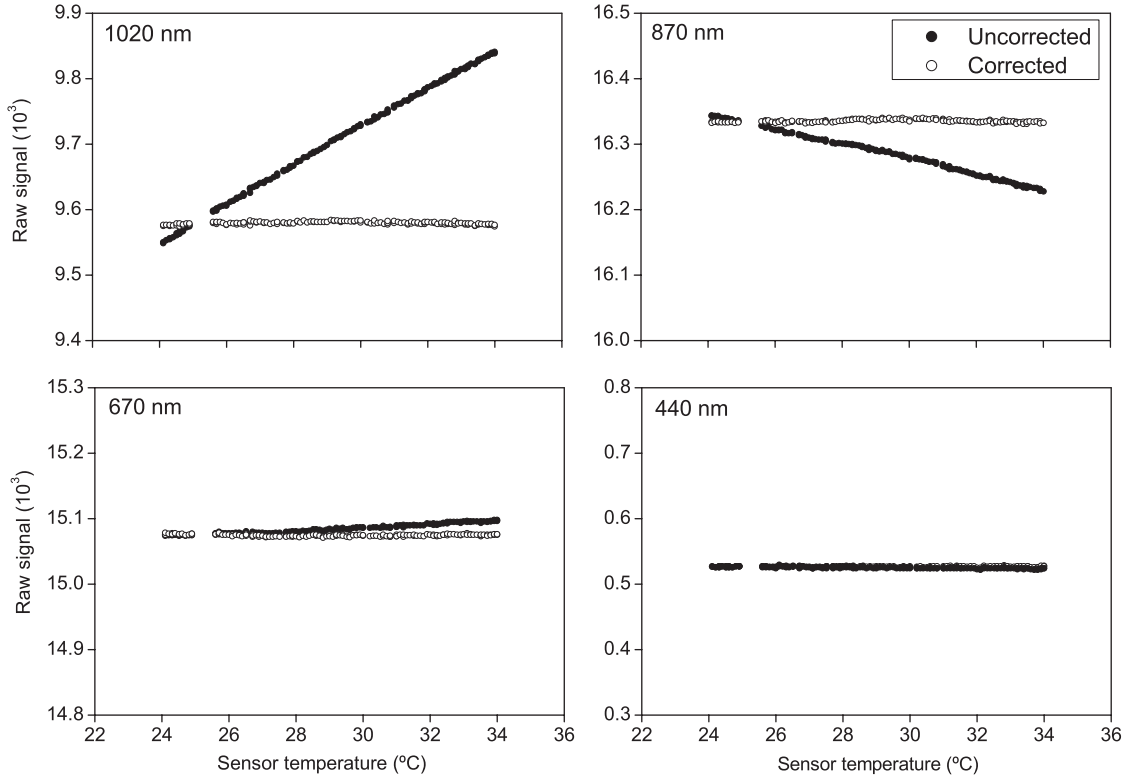

Fig. 4. Signal dependence on sensor temperature at the four wavelengths, defined through the comparison between uncorrected and corrected output signals.

of each filter may be simultaneously subject to appreciable thermal shift effects.

A. Dependence of Diffuse Radiance on Temperature

In the CIMEL used in the present study, the dependence of the measured diffuse radiance on the temperature was investigated through laboratory tests and then corrected. In particular, the radiance exiting a Bentham calibration sphere was measured by the radiometer, changing the room temperature throughout the range from 26 °C to 33 °C. As clearly shown in Fig. 4, the 1020 nm wavelength was found to be significantly affected by the temperature variation, whereas a less marked dependence was detected at the 870 nm wavelength. No evidence was found of significant variations in the measured signals as a function of the ambient temperature at both 670 and 440 nm wavelengths.

During the period in which the present data set was recorded, the laboratory tests were repeated three times, and the temperature coefficients were calculated in terms of percentage variations of the measured radiance per unit temperature change. Their values are shown in Table 3 for the two most sensitive wavelengths. At the 670 and 440 nm wavelengths, the laboratory tests were more difficult to perform. Thus the retrieved values of the temperature coefficients were not considered to be entirely reliable. Both the radiance exiting from the lamp and the sensitivity of the CIMEL sensor at the 440 nm wavelength assumed systematically very low values, making it difficult to determine temperature dependence correctly.

Although the values in Table 3 can be affected by appreciable experimental errors owing, for example, to the inhomogeneous heating of the optical sensor, filters, and temperature detector, the temperature coefficient at the 1020 nm wavelength was found to decrease from 2003 to 2004. Such year-to-year variations must be taken into account in the analysis of the V_0(1020 nm) time series. In fact, the entire radiance data set was corrected for the temperature dependence, using the coefficients retrieved in 2002. No update of the temperature coefficient was performed to correct the data recorded in 2003 and 2004. Such missed correction could have contributed to the apparent temperature dependence characterizing the last data set at 1020 nm wavelength.

Table 3. Values of the Temperature Coefficients for the Measured Diffuse Radiance

	Temperature Coefficients	
Measurement Period	870 nm	1020 nm
December 2002	$-0.07\%\ (°C)^{-1}$	$+0.29\%\ (°C)^{-1}$
April 2003	$-0.07\%\ (°C)^{-1}$	$+0.27\%\ (°C)^{-1}$
September 2004	$-0.08\%\ (°C)^{-1}$	$+0.21\%\ (°C)^{-1}$
AERONET geometry K	$-0.04\%\ (°C)^{-1}$	$+0.23\%\ (°C)^{-1}$
AERONET geometry A	$-0.007\%\ (°C)^{-1}$	$+0.26\%\ (°C)^{-1}$

At 870 nm wavelength, the temperature coefficient was considered to be extremely small, so the diffuse radiance measured at this wavelength was not corrected. No corrections were applied to the radiances measured at 670 and 440 nm. The temperature correction applied to the CIMEL radiometer in this work, is slightly different from the standard correction procedure performed by AERONET to the measurements taken by the network instruments similar to the example used in the present study. The temperature coefficients are derived by AERONET from laboratory tests for (i) three different temperature (T) ranges, $T < 21$ °C, 21 °C $\leq T < 32$ °C, and $T \geq 32$ °C, and (ii) for measurements taken at small angles from the lamp (<6°, called geometry A) and large angles (>6°, called geometry K). This is because in the above two cases the CIMEL takes measurements with the same sensor but using different gains. In this work the temperature coefficients, calculated for geometry K, were considered to be the same for both geometries.

Comparing the values retrieved here with those provided by AERONET[20] in the temperature range 21 °C $\leq T <$ 32 °C (Table 3), agreement was found with both the geometries at the 1020 nm wavelength. The 870 nm temperature coefficients were also found to be comparable with the values provided by AERONET for geometry K, even though no correction was applied in the present study at this wavelength. The fact that the measured radiance was corrected by using temperature coefficients retrieved for only one temperature range and not three temperature ranges, as in AERONET, could be a further reason for the temperature dependence found at the 1020 nm wavelength in Fig. 3.

B. Dependence of Direct Solar Irradiance on Temperature

It was not possible to perform a laboratory test to investigate the dependence of the measured direct solar irradiance on temperature. Therefore the irradiance measurements taken at the 1020 nm wavelength were corrected using the temperature correction coefficient per unit temperature variation $\Delta V/V = +0.25\%\ (°C)^{-1}$ suggested by Holben *et al.*[3] No corrections were applied at the other wavelengths in agreement with the standard temperature correction procedure performed by AERONET.

The SKYIL method uses both the diffuse radiance and the direct solar irradiance measurements to retrieve the values of $V_0(\lambda)$ because the normalized radiance $R(\lambda, \Theta)$ defined in Eq. (2) is processed routinely. Therefore it is reasonable to suppose that residual uncorrected temperature effects, induced by both the above quantities, can still be present on data and easily recognized in the retrieved time patterns of $V_0(\lambda)$, as shown in Fig. 3. To ascertain the suitability of these assumptions, a first step was performed by calculating the correlation coefficient between $V_0(\lambda)$ and temperature. According to the results shown in Table 4, a significant correlation was found on analyzing the subsets relative to the 1020 and 870 nm wavelengths, with a confidence level of 99% in both cases. At the 870 nm wavelength, an anticorrelated relationship was highlighted, in agreement with the decreasing trend of the corrected values of $R(\lambda, \Theta)$ versus the sensor temperature, as clearly shown in Fig. 4. Similarly, a slight anticorrelation (with a confidence level equal to 95%) was also found at the 440 nm wavelength, while that relative to the 670 nm wavelength was found to be very small (see Table 4).

Table 4. Values of the Correlation Coefficients between the Time Series of $V_0(\lambda)$ and the Sensor Temperature

	440 nm	670 nm	870 nm	1020 nm
Correlation coefficients	−0.14	0.015	−0.35	0.61

As a second step, a Fourier analysis was performed on the temperature time patterns to identify not only the yearly frequency (long wave) due to the seasonal temperature oscillation but also the frequency related to the diurnal component (short wave), which could affect the calculated values of $V_0(\lambda)$ since the SKYIL method retrieves two values of the solar calibration constant, one for the morning and one for the afternoon. The percentage difference between the extraterrestrial voltages computed using morning and afternoon selected data sets, was found to be on average equal to $(1 \pm 0.7)\%$ at the 440 nm wavelength and $(0.4 \pm 0.3)\%$ at the other wavelengths. Although the average differences fall closely within the threshold of the uncertainty of the method, they present a diurnal variability.

Although the selected data set was characterized by large scatter features, presenting irregularly spaced values of $V_0(\lambda)$, with temporal gaps of as much as 60 days in some cases, the Fourier analysis performed on the time series of $V_0(\lambda)$, relative to the 440, 870, and 1020 nm wavelengths, gave evidence of the presence of both the long- and short-wave frequency components. The short-wave component should have been smoothed after the application of the three-point moving average performed during the filtering of the data. Nevertheless, it was found to exist even after the moving procedure, due to the occurrence of a large number of temporal gaps. In fact, the moving average was applied on the data set (previously equispaced) by filtering only consecutive data (minimum two points) and without changing the isolated points.

The spectral analysis was not applied to the 670 nm series because no significant correlation with temperature was found, as shown in Table 4. In the other cases the time patterns of $V_0(\lambda)$ were assumed to consist of the following time-dependent terms:

$$V_0(t) = V_{0LONG} + V_{0SHORT} + V_{0RES} = A_L \sin(\omega_L t + \varphi_L) + A_S \sin(\omega_S + \varphi_S) + R(t), \quad (4)$$

where A_L, ω_L, and φ_L are the amplitude, the angular

frequency, and the phase of the long wave attributable to the seasonal oscillation, and A_S, ω_S, and φ_S are the same quantities relative to the short wave owing to the diurnal oscillation, respectively, while $R(t)$ is the residual term containing the other frequencies typical of the SKYIL method, as well as the trend of the time patterns.

It should be noted that the seasonal and diurnal components of V_0 can also be related to the seasonal and diurnal variations of minor external factors, such as NO_2 and O_3 absorption or daily fluctuations of relative humidity, which are all closely related to the temperature variations. To clean the signal V_0 from the V_{0LONG} and V_{0SHORT} terms, and then from the temperature and the other minor external factor effects, a generalized least-squares method was set up to (i) extract both the sinusoids from the detrended signal, (ii) calculate the weight of each oscillation term inside the original signal, and (iii) subtract the two terms by re-adding the trend. This analysis was applied to the entire data sets relative to the 440 and 870 nm wavelengths. At the 1020 nm wavelength, the analysis was limited to the period from 20 March 2003, onward. The reason for this choice is that the temperature dependence cannot be clearly spotted before this date, and the present method was found to fail when the two oscillation terms were extrapolated over the entire data set. This agrees with the fact that the omission of the update of temperature coefficients for the 2003 and 2004 measurements, as stated above, could favor the appearance of an oscillation in the data set relative to the period after 20 March 2003. The results are shown in Table 5.

At the 1020 nm wavelength, the seasonal component was found to include 58.2% of the total signal, whereas the diurnal component was evaluated to be 9.4% of the signal previously cleaned by the long-wave effects. Thus 67.6% of the time variations in $V_0(\lambda)$ with wavelength $\lambda = 1020$ nm were estimated to be attributable to temperature-dependence effects, although the normalized radiance $R(\lambda, \Theta)$ was considered to be properly corrected for both direct and diffuse irradiance components. The reason for a wrongly corrected signal may be due to (i) the ignored update of the temperature coefficients for the diffuse irradiance data taken after 20 March 2003, (ii) the use of a temperature coefficient independent of temperature within the measurement range, and (iii) an unrealistic correction of direct irradiance.

With regard to the latter quantity, evidence of the temperature dependence of the aerosol optical thickness retrieved from only direct irradiance measurements was found by Campanelli *et al.*,[21] who examined simultaneous measurements taken with a CIMEL and a PREDE Sun–sky radiometer, regularly thermostated. Evaluating the difference between the correlation coefficients calculated by relating each set of aerosol optical thickness to the measured external temperature, the measure of the temperature dependence for the CIMEL was estimated. The dependence features were found to be particularly marked at the 440 and 870 nm wavelengths and weak at only the 1020 nm wavelength, although an appropriate correction procedure[3] was applied at the last wavelength.

Variations in the solar calibration constants with temperature clearly depending on wavelength were also found by von Hoyningen-Huene[22] validating satellite measurements through the use of AERONET data. Estimates of the growing coefficient K of $V_0(\lambda)$ per unit increase of temperature were obtained by this author at various wavelengths. He found that the temperature dependence decreases appreciably as the wavelength increases from 440 to 870 nm, but becomes stronger at 1020 nm, presenting values of $K = 0.01$, 0.004, 0.002, and 0.004 $(°C)^{-1}$ at the 440, 670, 870, and 1020 nm wavelengths, respectively.

Consequently, in spite of the use of the suggested correction, the existence of further temperature dependence effects on the direct irradiance cannot be excluded. Thus the 2002 data set relative to the 1020 nm wavelength should also be submitted to spectral analysis, in order to extrapolate the long- and short-wave components. The application of the above method allowed the retrieval and correction of the data for this time period, for a seasonal component that was evaluated to be 25.8% of the overall signal, and for a diurnal component of 0.9%, which is in practice negligible.

With regard to the 870 nm wavelength, the long-wave contribution to the signal was found to be equal to 20.7%, and, hence, lower than that determined at the 1020 nm wavelength for the 2003–2005 data set, whereas the short-wave contribution was estimated to be 7.2% and, therefore, quite comparable with that found at 1020 nm. At this wavelength, approximately

Table 5. Values of the Amplitude, Phase, and Weight of the Seasonal (Long-Wave) and Diurnal (Short-Wave) Components at the Three Analyzed Wavelengths

	1020 nm				870 nm		440 nm	
	Long Wave		Short Wave		Long Wave	Short Wave	Long Wave	Short Wave
Amplitude [volt]	46.6[a]	17.5[b]	9.3[a]	2[b]	36.7	13.8	26.9	9.3
Phase [rad]	2.6[a]	4.3[b]	1[a]	1[b]	0.2	1	0.3	1.4
Weight [%]	58.2[a]	25.8[b]	9.4[a]	0.9[b]	20.7	7.2	7.8	2.3

[a]Data only from 20 March 2003 to March 2005.
[b]Data from early January 2002 to 20 March 2003.

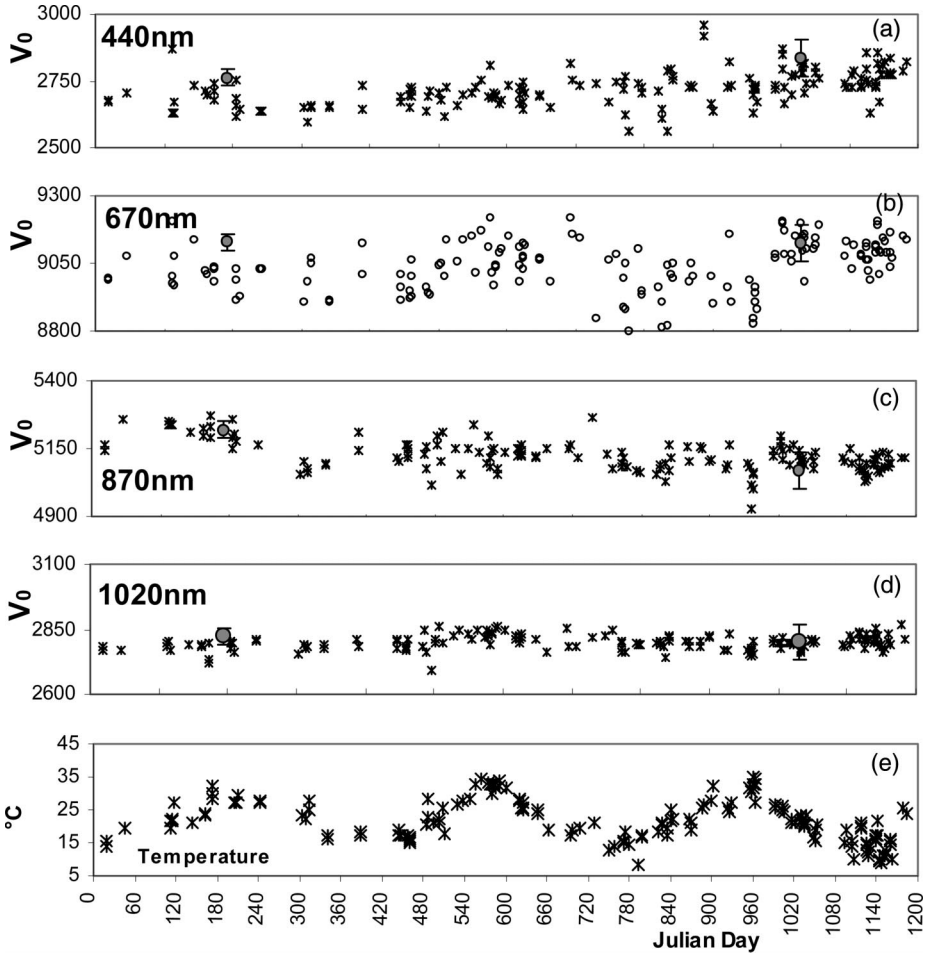

Fig. 5. Time patterns of the calibration constant $V_0(\lambda)$ at the four wavelengths after the temperature correction. Data shown in (c) relative to the 670 nm wavelength are not corrected. The solid symbols with error bars represent the experimental calibration values of $V_0^{exp}(\lambda)$. (e) Time patterns of the temperature inside the instrument. The origin of the Julian day axis is set at 1 January 2002.

28% of the signal was evaluated to be attributable to temperature dependence effects.

As expected, the signals taken at the 440 nm wavelength were found to be even less affected by temperature dependence effects, since the overall weight of long- and short-wave components amounts to 10.1%.

The corrected signals are plotted in Fig. 5, and the accuracy of the method calculated after the temperature correction is given in Table 2. To validate the method proposed here, the calibration values retrieved by SKYIL can be compared with the experimental values of $V_0^{exp}(\lambda)$ given in Table 1. The validation consists of the two following steps: (i) comparison of the general trend of the calibration constant time patterns and (ii) comparison among their absolute values. With regard to the first step, the trend of $V_0^{exp}(\lambda)$ was estimated at each wavelength by examining the experimental data and then determining the slope of the line connecting two available points (m_{exp}). The uncertainty of the retrieved trend was calculated following the method of the minimum and maximum slope coefficients of the fitted line, taking into account the errors affecting the values of $V_0^{exp}(\lambda)$ listed in Table 1.

The trend of V_0 determined at each wavelength using the SKYIL method (m_{sky}) was estimated by defining the slope of the regression line for the data set taken only on the days from 23 July 2002 to 17 October 2004, i.e., on days within the two experimental calibration dates. The results are shown in Table 6. The increasing trend recorded by m_{exp} at the

Table 6. Trend of the Calibration Constants Obtained for the Experimental Values (m_{exp}) and the Values Retrieved by the SKYIL Method (m_{sky})[a]

Wavelength λ (nm)	Trend	
	$m_{exp} \pm \Delta m_{exp}$	$m_{sky} \pm \Delta m_{sky}$
440	0.090 ± 0.045	0.120 ± 0.003
670[b]	−0.007 ± 0.055	0.054 ± 0.001
870	−0.178 ± 0.023	−0.071 ± 0.001
1020	−0.024 ± 0.003	−0.002 ± 0.001

[a]Data obtained after the use of the temperature correction procedure to analyze the data relative to all the wavelengths, except 670 nm.

[b]The data relative to the 670 nm wavelength are not corrected for temperature effects.

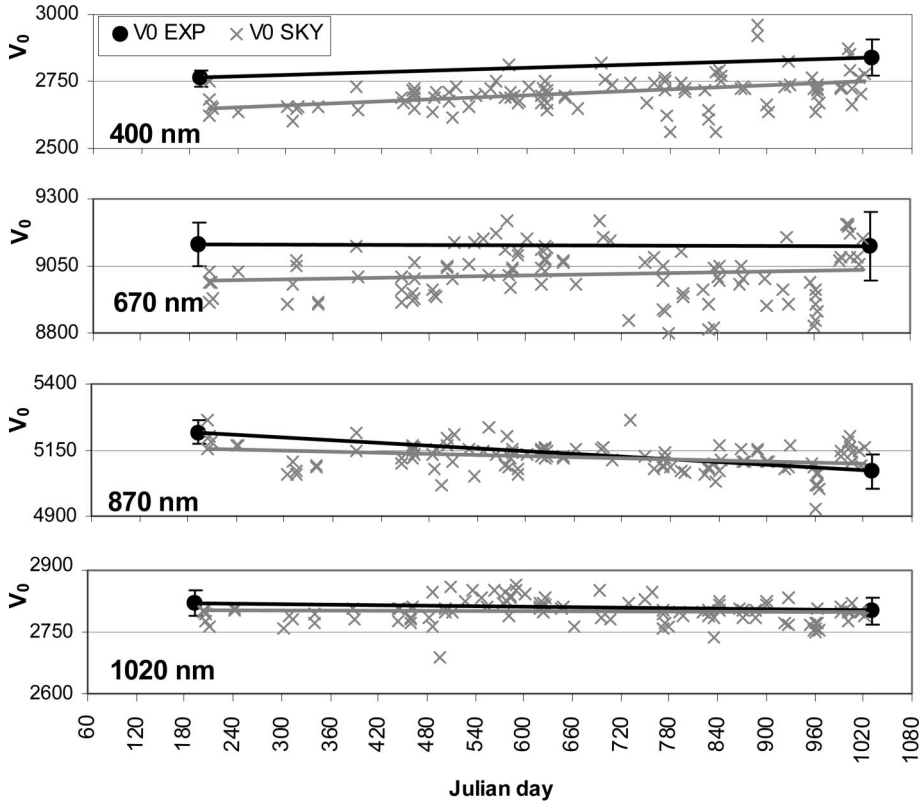

Fig. 6. Time patterns of the calibration constants $V_0(\lambda)$ at the four wavelengths, obtained after the application of the temperature correction to the data relative to the period limited by the two experimental calibration dates. Data pertaining to the 670 nm wavelength were not corrected. The gray line represents the corresponding regression line, m_{sky}. The solid symbols with error bars represent the experimental calibration values V_0^{exp}. The solid black line represents the corresponding regression line m_{exp}. The origin of the Julian day axis is set at 1 January 2002.

440 nm wavelength was found to be consistent with m_{sky}, within the experimental error, and the nearly stable behavior at the 670 nm wavelength was also well reproduced. At the 870 nm wavelength, the negative trend turns out to be defined by both m_{exp} and m_{sky}, but it is slightly underestimated using the SKYIL method. This seems mainly attributable to the poor agreement between the second V_0^{exp} calibration value and the V_0 SKYIL values retrieved in October 2004 as shown in Fig. 6. Even in the case of the 1020 nm wavelength, the decreasing trend is recognized by both m_{exp} and m_{sky} although it again turns out to be slightly underestimated with respect to the previous case, because of the poor agreement between the first V_0^{exp} value and the V_0 SKYIL calibrations retrieved in July 2002 as can be seen in Fig. 6. However, it must also be taken into account that the slopes of both regression lines found at this wavelength are very small and presumably not related to a real instrumental drift.

Examining the comparison between the absolute values of V_0^{exp} and V_0 retrieved by the SKYIL method, the agreement quality cannot be evaluated directly without an accurate selection, at each wavelength, of the values of $V_0(\lambda)$ located at approximately $V_0^{exp}(\lambda)$. In fact, comparing the values of $V_0^{exp}(\lambda)$ with the closest values of $V_0(\lambda)$ is not a correct procedure, princi-

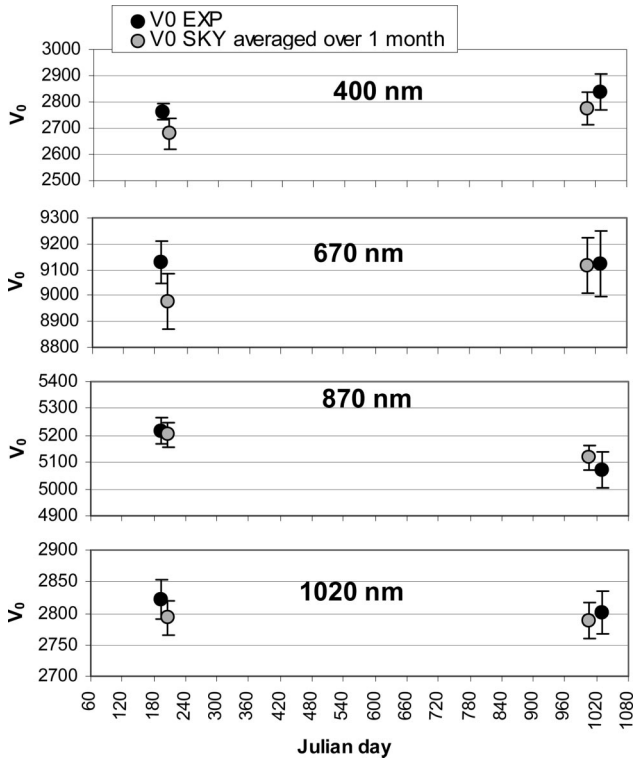

Fig. 7. Time patterns of the calibration constants $V_0^{exp}(\lambda)$ and $V_0^{Sky}(\lambda)$ at the four wavelengths.

Table 7. Absolute Percentage Differences between the Values of $V_0^{exp}(\lambda)$ and $V_0^{Sky}(\lambda)$ at the Four Wavelengths

Wavelength (nm)	Absolute Values of the Percentage Difference (%)	
	2002 Data Set	2004 Data Set
440	3.0	2.2
670	1.7	0.1
870	0.3	0.1
1020	1.0	0.5

pally because (i) the time patterns of $V_0(\lambda)$ provided by SKYIL do not follow a linear trend but frequently exhibit some short-time variations related to the method itself, which can distort the comparison in particular cases, and (ii) the dates of the two calibration constants are only nominal, because the intercomparison transfer test was performed using data from 8 July to 11 July 2002, for the first calibration (having 11 July as a nominal date) and from 27 September to 25 October 2004, for the second calibration (with a nominal date fixed at 25 October). Thus it was decided to compare each value of $V_0^{exp}(\lambda)$ with a value of $V_0(\lambda)$ obtained as the average calculated over the SKYIL available points determined within one month around the experimental date, that is, 15 days before and 15 days after the experimental date. The results are labeled with symbols $V_0^{Sky}(\lambda)$. The uncertainty affecting the results provided by the SKYIL method, as retrieved in Table 2 after the use of the correction procedure, was assumed to be the measure of the uncertainty on V_0^{Sky}. The choice of the above time interval seems to be reasonable, since a significant change in the solar calibration constant is unlikely within a limited time interval of only one month. The results are shown in Fig. 7 and Table 7.

In all cases, the values of V_0^{exp} and V_0^{Sky} were found to be comparable within their uncertainties, although greater differences have been observed in the 2002 calibration findings at all the wavelengths. The most apparent disagreement was found at the 440 nm wavelength, equal to 3% in 2002 and 2.2% in 2004. A possible explanation for such discrepancies could be that this wavelength is more sensitive to the scattering effects produced by clouds than the others. Even if the cloud screening performed on the present data sets was estimated to be capable of rejecting the data taken with clouds in front of the Sun or around the Sun, the presence of cirrus or other clouds in sky sectors far from the observation point of the instrument could corrupt the direct irradiance measurements performed at this wavelength. Moreover effects attributable to the NO_2 absorption could also be present at this wavelength.

The other marked disagreement recognizable for the 2002 calibration at the 670 nm wavelength could be related to the fact that the intercomparison transfer test for the determination of V_0^{exp} at this wavelength was performed between two instruments having slightly different transmission peak wavelengths of 674 nm for the master instrument No. 307 and 670 nm for the field instrument.

5. Sensitivity Study

The first sensitivity study was carried out to demonstrate that the method does not depend on the assumed first guess $V_0^0(\lambda)$. For this purpose a slightly different elaboration procedure was set up. As shown in Fig. 2, for each day considered in the analysis, the value of $V_0(\lambda)$ retrieved on the previous day was used as a first guess, except for the first day of the data set in which the experimental calibration constants $V_0^{exp}(\lambda)$ were used as $V_0^0(\lambda)$ inputs. The independence of the first guess can be carefully checked by arbitrarily changing the first guess and then analyzing the retrieved final values, but with this elaboration procedure it can be done by varying only the input calibration of the first day of the data set. Considering each day separately and processing each daily data set using the same first guess in place of the value retrieved from the previous day, the independence can be checked using the entire data set. Following this criterion, the data set was divided into two parts, the first from early January 2002 to 14 September 2003, and the second from 15 September 2003 to March 2005. Subsequently for each day the values of $V_0^{exp}(\lambda)$ relative to 2002 and 2004 and given in Table 1 were used as a first guess, respectively. The procedure was repeated by increasing and decreasing the constants $V_0^0(\lambda)$ by 0.1%, 10%, and 20%. All the series were selected, as in the previous section, for an inversion

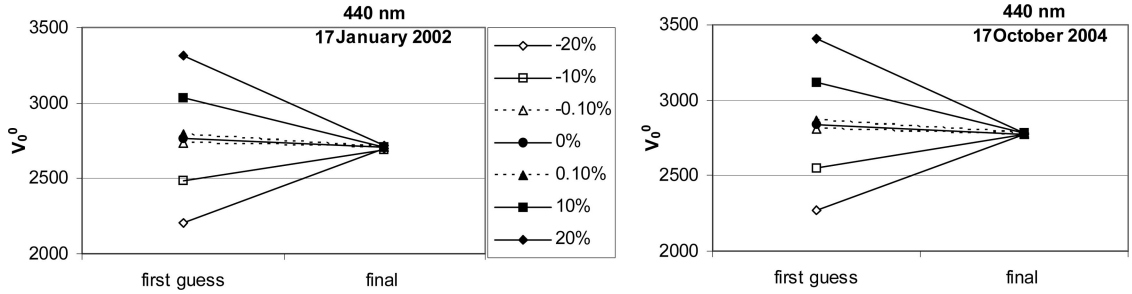

Fig. 8. Final values of the calibration constant V_0(440 nm), as retrieved on two measurement days after the application of the SKYIL method for several first guesses obtained by increasing and decreasing the original value (0% in the legend) by 20%, 10%, and 0.1%.

Table 8. Mean Percentage Dependence of Constant $V_0(\lambda)$ on the Real and Imaginary Parts of Particulate Refractive Index $n - ik$, Obtained through an Averaging Procedure over the Entire Data Set

		440 nm	670 nm	870 nm	1020 nm
Present data set	Dependence on n (%)	1.02 ± 1.09	0.31 ± 0.31	0.22 ± 0.22	0.24 ± 0.22
	Dependence on k (%)	0.46 ± 0.42	0.13 ± 0.13	0.12 ± 0.11	0.15 ± 0.15
		400 nm	500 nm	870 nm	1020 nm
Campanelli *et al.* (Ref. 10)	Dependence on n (%)	1.29 ± 0.90	0.80 ± 0.79	0.61 ± 0.83	0.57 ± 0.78
	Dependence on k (%)	0.85 ± 0.98	0.35 ± 0.38	0.29 ± 0.45	0.25 ± 1.95

accuracy higher than 5%, for $\tau(440\text{ nm}) < 0.3$, and according to the Chauvenet criterion.[17]

The results found at the 440 nm wavelength on two measurement days are shown in Fig. 8. It is evident that the method converges toward very close final values, independent of the first guess. In particular, the mean percentage discrepancies among the retrieved final values were found to be equal to 0.2%, 0.05%, 0.03%, and 0.02% at the 440, 670, 870, and 1020 nm wavelengths, respectively, clearly within the uncertainty limits of the method. Such differences were calculated with respect to the final value retrieved using the values of $V_0^0(\lambda)$ associated with null increase. The convergence was reached at the third loop even in the worst cases.

The second sensitivity analysis aimed to study the dependence of the retrieval procedure on the assumed refractive index of particulate matter. The SKYIL method retrieves the calibration constant assuming a fixed value of the complex refractive index to calculate the spectral values of aerosol extinction optical thickness. Campanelli *et al.*[10] demonstrated that the method can depend closely on (i) the imaginary part k to an extent not exceeding 1.8% at $\lambda = 400$ nm, and 0.5% at $\lambda = 1020$ nm, and (ii) the real part n to an extent within 2.2% at $\lambda = 400$ nm, and 1.4% at $\lambda = 1020$ nm, as can be seen in Table 8. However, these sensitivity features were determined by using different filtering criteria, in contrast to the procedure adopted in the present study and explained in Section 3. In the present case, by adopting more severe selection criteria, the sensitivity was calculated to ascertain whether the dependence on the assumed refractive index is really consistent with the method's uncertainty. The sensitivity to n was studied by applying the SKYIL method for an assumed value of $k = 0.005$ and several values of n equal to 1.35, 1.50, and 1.65. For each day of the selected data set, the STD relative to $V_0(\lambda)$ was retrieved for all the above values of n, and the percentage relative errors were calculated. A similar procedure was followed to evaluate the dependence of $V_0(\lambda)$ on the imaginary part k, using a fixed value of $n = 1.50$ and several values of k equal to 0, 0.005, and 0.03. The results are shown in the first two rows of Table 8. The maximum dependence on n was 2.1% at 440 nm, decreasing to 0.5% at both 870 and 1020 nm, whereas the maximum variability on k was found to be of 0.9% at 440 nm, 0.2% at 870 nm, and 0.3% at 1020 nm. All these values are within the method's uncertainty. Therefore it can be stated that the sensitivity of the SKYIL method to the assumed refractive index is also negligible. Moreover, in both the analysis procedures followed to define the dependence features on n and k, the percentage dependence was evaluated to be smaller than the those retrieved by Campanelli *et al.*,[10] presumably as a result of the stricter selection of the values of $V_0(\lambda)$ adopted in the present study.

6. Conclusions

The SKYIL method is a well-tested *in situ* procedure for the daily determination of the solar calibration constants, specifically created for the PREDE Sun–sky radiometers. It was applied to a CIMEL instrument located in Valencia, Spain, not belonging to the AERONET network, taking into account the different mechanical and electronic characteristics of the two radiometers. For this reason, the SKYIL method was adapted to the characteristics of the CIMEL instrument, bearing in mind that it is suitable for application only if the radiometer has previously been calibrated using a standard lamp for the diffuse radiance. The iterative procedure for the determination of the solar calibration constants was applied to a 3-year data set, and the results were compared with the two available sets of experimental calibration constants determined during this period with the standard Langley plot method. To improve the accuracy of the method, a more severe selection of the retrieved values of $V_0(\lambda)$ was performed, as compared with the qualified selection made by Campanelli *et al.*[10] In particular, all the values retrieved during days characterized by high atmospheric turbidity conditions were rejected, and the method followed to filter the short-term variations related to the SKYIL findings was appreciably improved.

A marked influence of the external temperature on the retrieved time patterns of the calibration constants was highlighted. Since the SKYIL method uses both diffuse radiance and direct solar irradiance measurements to retrieve the values of $V_0(\lambda)$, the temperature dependence effects induced by both these irradiance components have been clearly identified in the retrieved time patterns of $V_0(\lambda)$. The temperature dependence of the diffuse radiance measured at 1020 nm was investigated through laboratory tests and subsequently corrected. The direct solar irradiance measurements taken at the same wavelength were also corrected following the Holben *et al.*[3] procedure. In spite of these corrections, the correlation coefficients

calculated between $V_0(\lambda)$ and the measured temperature showed evidence of residual temperature effects at all the wavelengths except 670 nm. The use of a Fourier analysis allowed the definition of a yearly frequency owing to the seasonal temperature oscillations, as well as a diurnal component, both relative to the 440, 870, and 1020 nm wavelengths. Subsequently, a generalized least-squares method was set up to remove the two components from the values of $V_0(\lambda)$. The analysis established that percentages of approximately 68%, 28%, and 10% of the total signal can be attributed to temperature dependence effects at the 1020, 870, and 440 nm wavelengths, respectively.

It should be made clear that the analysis of the temperature dependence is not a part of the SKYIL method. During the present study, it was necessary to perform such analysis because the results obtained by applying the SKYIL method to the CIMEL data, without AERONET temperature corrections, were found to be of worse quality than those obtained when the method was applied to a PREDE instrument,[10] which does not require any temperature correction. The procedure set up in this study to correct the temperature dependence certainly requires further investigation. Nevertheless, the SKYIL method was evaluated to give very good results, when tested on the AERONET database, which is accurately corrected for temperature dependence.

Once the temperature correction was performed, the accuracy of the method was evaluated, finding that it is within 2.1% and 1.0%, depending on wavelength. The improvement of the accuracy with respect to the previously retrieved values[10] is an important result since the nominal uncertainty affecting the values of $V_0(\lambda)$ given by the AERONET calibration method (of 1%–2%) and the uncertainty produced by the SKYIL method turn out to be more similar in the present case.

The time trend of the calibration constant values retrieved by the SKYIL method was compared with that calculated in the two experimental calibrations. The agreement was consistent with the experimental errors at the 440 and 670 nm wavelengths. At 870 nm and 1020 nm, a negative trend was defined using both the experimental calibrations and the SKYIL method, although slightly underestimated in the latter case.

A comparison was also performed between the values of the calibration constants found from the two experimental calibrations and the values of $V_0(\lambda)$ retrieved following the SKYIL method, averaged over a 1-month period centerd on the two experimental calibration dates. At all the wavelengths, the values of $V_0^{exp}(\lambda)$ and $V_0^{Sky}(\lambda)$ were found to be comparable, within their uncertainties.

Finally, a study was performed to define the dependence features of the results on the first guess $V_0^0(\lambda)$ and on the assumed refractive index. It is true that the present analysis does not take into account the possible dependence on numerous input parameters and assumptions, which are implicit in a radiative transfer model, such as those concerning the surface albedo and the choice of the overall size range of the particle volume size distribution used in the SKYRAD code.[5] However, the first guess $V_0^0(\lambda)$ and the refractive index were considered to be the most important causes of uncertainty. In both cases the variability was found to be consistent with the uncertainty of the method.

In conclusion, the SKYIL method was found to be suitable for use to determine the solar calibration constants also for CIMEL instruments, provided that the radiometer has been previously calibrated for the diffuse radiance. A further step of the present investigation will be the application of the method to a CIMEL Sun–sky radiometer belonging to the AERONET network. A calibration method independent of the AERONET system would be very useful to diagnose the condition of a sky radiometer, whose data analysis is sensitive to small errors in the measured data. Using an independent method the variation of the calibration constant attributable to instrumental drift can be quickly identified, so that appropriate corrections can be applied to data, starting exactly from the period in which the deviation occurred.

Before this step, several problems must be resolved. First, the measured values of direct solar irradiance (not provided on the AERONET web site) need to be retrieved from the aerosol optical thickness values that can be downloaded directly from the web. To perform this inversion, all the corrections applied following the AERONET protocol for the calculation of the aerosol optical depth from direct solar irradiance measurements need to be well known. A further problem is that the SKYIL method needs at least eight measurements in the almucantar geometry performed on the same day. The instrument used in the present analysis has been implemented for more than 30 almucantar measurements per day since it does not belong to the AERONET network, but the standard schedule for network Sun–sky radiometers usually leads to eight to ten almucantar measurements per day. This number of measurements can be drastically lowered after the application of the cloud screening, spoiling the application of the SKYIL method. Currently, the only way of overcoming this drawback is to use instruments located at sites where the meteorological conditions ensure a less frequent presence of clouds around the Sun.

Although limited to only one instrument, the present study furnished interesting results. For these reasons, it is worthwhile to continue investigations for better application of the SKYIL method to the AERONET database. Simultaneously, the application of the present methodology is recommended for CIMEL instruments involved in other networks, such as the recently created Spanish network RIMA. Furthermore these instruments should be employed, performing a greater number of experimental calibration tests, for both direct and diffuse solar irradiance, thus improving the validation of the SKYIL method.

The authors dedicate this work to the memory of their colleague and friend Yoram Kaufman. He never failed to prove his scientific generosity, and during his last visit in Rome he made important suggestions for the development of the present work, always with his spontaneous intellectual honesty.

The authors thank Brent Holben and Ilya Slutsker of the AERONET project for their comments, which resulted in a substantial improvement of this work.

This research was supported by the strategic Fondo Integrativo Speciale per la Ricerca program Sustainable Development and Climate Changes sponsored by the Italian Ministry of University and Scientific Research (MIUR) and developed in the framework of the cooperative project between the CNR and MIUR, Study of the Direct and Indirect Effects of Aerosols and Clouds on Climate (AEROCLOUDS).

References

1. Y. J. Kaufman, D. Tanré, and O. Boucher, "A satellite view of aerosols in the climate system," Nature **419,** 215–223 (2002).
2. T. Takamura and T. Nakajima, "Overview of SKYNET and its activities," Opt. Pura Apl. **37,** 3303–3308 (2004).
3. B. N. Holben, T. F. Eck, I. Slutsker, D. Tanré, J. P. Buis, A. Setzer, E. Vermote, J. A. Reagan, Y. Kaufman, T. Nakajima, F. Lavenu, I. Jankowiak, and A. Smirnov, "AERONET-A federated instrument network and data archive for aerosol characterization," Remote Sens. Environ. **66,** 1–16 (1998).
4. T. Nakajima, M. Tanaka, and T. Yamanouchi, "Retrieval of the optical properties of aerosols from the aureole and extinction data," Appl. Opt. **22,** 2951–2959 (1983).
5. T. Nakajima, G. Tonna, R. Rao, P. Boi, Y. Kaufman, and B. Holben, "Use of sky brightness measurements from ground for remote sensing of particulate polydispersions," Appl. Opt. **35,** 2672–2686 (1996).
6. O. Dubovik and M. D. King, "A flexible inversion algorithm for retrieval of aerosol optical properties from sun and sky radiance measurements," J. Geophys. Res. **105,** 20673–20696 (2000).
7. O. Dubovik, B. N. Holben, T. Lapyonok, A. Sinyuk, M. I. Mishchenko, P. Yang, and I. Slutsker, "Nonspherical aerosol retrieval method employing light scattering by spheroids," Geophys. Res. Lett. **29,** doi:10.1029/2001GL014506 (2002).
8. World Meteorological Organization/Global Atmosphere Watch, "Workshop on a global surface-based network for long-term observations of column aerosol optical properties," GAW Rep. 162, WMO TD 1287, Davos, 8–10 March 2004 (2005).
9. B. N. Holben, "AERONET workshop and Steering Committee Review, May 10–14, 2004," Opt. Pura Apl. **37,** 3001–3075 (2004).
10. M. Campanelli, T. Nakajima, and B. Olivieri, "Determination of the solar calibration constant for a sun–sky radiometer: Proposal of an *in situ* procedure," Appl. Opt. **43,** 651–659 (2004).
11. G. E. Shaw, "Error analysis of multi-wavelength sun photometry," Pure Appl. Geophys. **114,** 1–14 (1976).
12. V. Estellés, "Characterization of the atmospheric aerosols at Valencia by means of sunphotometry," Ph.D. dissertation (Universitat de València, 2006) (in Spanish).
13. A. Smirnov, B. N. Holben, T. F. Eck, O. Dubovik, and I. Slutsker, "Cloud screening and quality control algorithms for the AERONET database," Remote Sens. Environ. **73,** 337–349 (2000).
14. V. Estellés, M. P. Utrillas, J. L. Gómez-Amo, R. Pedrós, and Martínez-Lozano, "Aerosol size distributions and air mass back trajectories over a mediterranean coastal site," Int. J. Remote. Sens. **25,** 39–50 (2004).
15. V. Estellés, M. P. Utrillas, J. A. Martínez-Lozano, A. Alcántara, L. Alados-Arboledas, F. J. Olmos, J. Lorente, X. de Cabo, V. Cachorro, H. Horvath, A. Labajo, M. Vilaplana, J. P. Díaz, A. M. Díaz, A. M. Silva, T. Elías, M. Pujadas, J. A. Rodríguez, J. Cañada, and Y. García, "Intercomparison of spectroradiometers and sun photometers for the determination of the aerosol optical depth during the VELETA2002 field campaign," J. Geophys. Res. **111,** D17207, doi:1029/2005;D006097 (2006).
16. L. Alados-Arboledas, J. Lorente, J. A. Martínez-Lozano, V. Cachorro, A. Labajo, B. de la Morena, J. P. Díaz, M. Pujadas, H. Horvath, A. M. Silva, G. Pavese, and J. Rodríguez, "VELETA 2002 field campaign," Geophysical Research Abstracts **5,** 12218 (2003).
17. H. D. Young, *Statistical Treatment of Experimental Data* (McGraw-Hill, 1962), pp. 78–80.
18. C. A. Gueymard, "Parameterized transmittance model for direct beam and circumsolar spectral irradiance," Sol. Energy **71,** 325–346 (2001).
19. C. Wehrli, *Extraterrestrial Solar Spectrum,* Publ. No. 615 (World Radiation Center, Davos, 1985).
20. B. Holben and I. Slutsker, NASA Goddard Space Flight Center, Greenbelt, Md., USA (personal communication, 2006).
21. M. Campanelli, G. Gobbi, C. Tomasi, and T. Nakajima, "Intercomparison between aerosol characteristics retrieved simultaneously with CIMEL and PREDE sun–sky radiometers in Rome, Torvergata AERONET site," Opt. Pura Apl. **37,** 3159–3164 (2004).
22. W. von Hoyningen-Huene, University of Bremen, Institute of Environmental Physics, Otto-Hahn-Allee, 28359 Bremen, Germany (personal communication, 2006).